

See discussions, stats, and author profiles for this publication at: <https://www.researchgate.net/publication/274087730>

# Direct Evidence for Secondary Interactions in Planar and Non-Planar Aromatic $\pi$ -Conjugates and Their Photophysical Characteristics in Solid State Assemblies.

ARTICLE *in* THE JOURNAL OF PHYSICAL CHEMISTRY B · MARCH 2015

Impact Factor: 3.3 · DOI: 10.1021/acs.jpcb.5b01956 · Source: PubMed

---

CITATION

1

READS

293

## 3 AUTHORS, INCLUDING:



Karnati Narsimha

Indian Institute of Science Education and Res...

3 PUBLICATIONS 7 CITATIONS

[SEE PROFILE](#)



Manickam Jayakannan

Indian Institute of Science Education and Res...

74 PUBLICATIONS 1,566 CITATIONS

[SEE PROFILE](#)

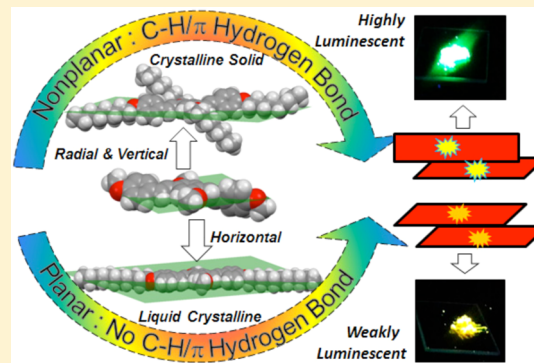
# Direct Evidence for Secondary Interactions in Planar and Nonplanar Aromatic $\pi$ -Conjugates and Their Photophysical Characteristics in Solid-State Assemblies

Mahima Goel, Karnati Narasimha, and Manickam Jayakannan\*

Department of Chemistry, Indian Institute of Science Education and Research (IISER), Dr. Homi Bhabha Road, Pune 411008, Maharashtra, India

## Supporting Information

**ABSTRACT:** Direct evidence for non-covalent secondary interactions in planar and nonplanar aromatic  $\pi$ -conjugates and their solid-state assemblies is established. A series of horizontally, vertically, and radially expanded oligo(phenylenevinylene)s (H-OPVs, V-OPVs, and R-OPVs, respectively) were designed with a fixed  $\pi$ -core and variable alkyl chain lengths on the periphery. Single-crystal structures of the OPVs were resolved to trace the secondary interactions that direct the solid-state self-organization and molecular packing of the chromophores. The H-OPVs were found to be planar, and they did not show any secondary interactions in the crystal lattices. The V-OPVs and R-OPVs were found to be nonplanar and to exhibit multiple CH/ $\pi$  hydrogen-bonding interactions among aryl hydrogen donors and acceptors. The enthalpies of the melting and crystallization transitions revealed that the planar H-OPVs are highly crystalline compared with the nonplanar R-OPVs and V-OPVs. Polarized light microscopy studies revealed the formation of one-dimensional nematic mesophases in H-OPVs. The absolute solid-state photoluminescence quantum yields (PLQYs) of the OPVs were determined using an integrating sphere setup. The highly packed H-OPVs showed low PLQYs compared with those of the weakly packed V-OPVs and R-OPVs. Time-resolved fluorescence decay measurements revealed that the excited-state decay dynamics of highly packed H-OPVs was much faster with respect to their low PLQYs. The decay profiles were found to be relatively slow (with higher life time ( $\tau$ )) in the V-OPVs and R-OPVs. A field-effect transistor (FET) device was constructed for an OPV sample that showed a hole carrier mobility in the range of  $10^{-5}$  cm $^2$  V $^{-1}$  s $^{-1}$ . The present investigation thus provides a new opportunity to trace the role of secondary interactions on  $\pi$ -conjugated mesophase self-assemblies and their solid-state emission and FET devices, more specifically based on OPV chromophores.



## INTRODUCTION

Secondary interactions are important driving forces in the precise three-dimensional molecular arrangements of organic  $\pi$ -conjugated chromophores in electronic devices such as light-emitting diodes,<sup>1</sup> photovoltaics,<sup>2</sup> field-effect transistors (FETs),<sup>3</sup> etc. Thin-film FETs materials such as pentacene and acenes,<sup>4–6</sup> oligothiophenes,<sup>7–9</sup> fused thiophene aromatics,<sup>10,11</sup> and tetrathiafulvalenes<sup>12,13</sup> were reported to exhibit either a face-to-face or face-to-edge orientation as the most preferred configuration in the solid state. Surprisingly, these planar  $\pi$ -conjugates did not show any  $\pi$ – $\pi$  stacking as expected in the crystal lattices.<sup>6,10</sup> Recent studies revealed that nonplanarity was observed in the aromatic cores of phenylene, naphthalene, and anthracene rings irrespective of the topology, size, and nature of the substitution.<sup>14,15</sup> Non-covalent interactions such as CH/ $\pi$ <sup>16,17</sup> and RCH<sub>2</sub>O/ $\pi$ <sup>18–20</sup> (R = H or alkyl) were reported to stabilize the packing of  $\pi$ -conjugated chromophores. Large numbers of  $\pi$ -conjugated materials belonging to phenylenevinylenes, fluorenes, and low-band-gap materials were found to be sluggish to produce good-quality

single crystals. This leads to a larger ambiguity in establishing the correlation among various factors such as molecular planarity, types of non-covalent secondary interactions, packing abilities, and photophysical and charge mobility characteristics of  $\pi$ -conjugated materials in general.<sup>4</sup>

Liquid-crystalline (LC) mesophase assemblies of  $\pi$ -conjugated chromophores represent an emerging approach for optoelectronic applications.<sup>21–23</sup> In this approach, the chromophores can be easily aligned thermotropically on desired substrates (e.g., a glass plate) by means of a solvent-free melt crystallization process. Optimization of the LC active temperature window to get the right fluid states of the mesogens, LC morphologies, and structure–property relationships are some of the issues yet to be addressed in  $\pi$ -conjugated LC materials.<sup>23</sup> For the past few years, our group has devoted effort to the study of  $\pi$ -conjugated LC mesophase assemblies of

Received: February 27, 2015

Revised: March 23, 2015

Published: March 24, 2015

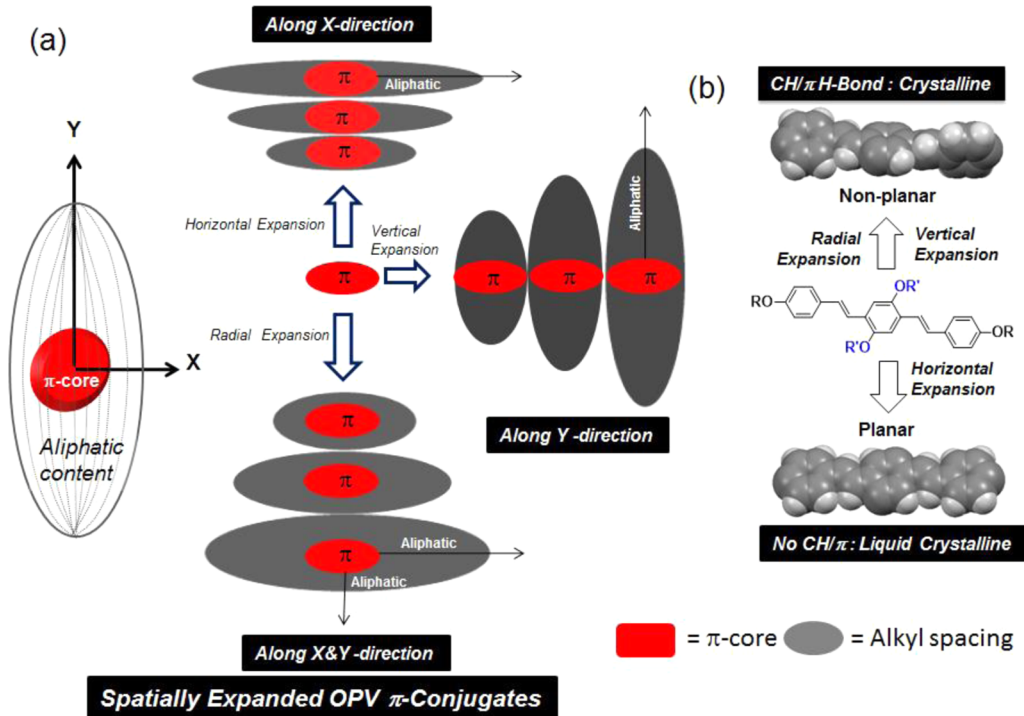
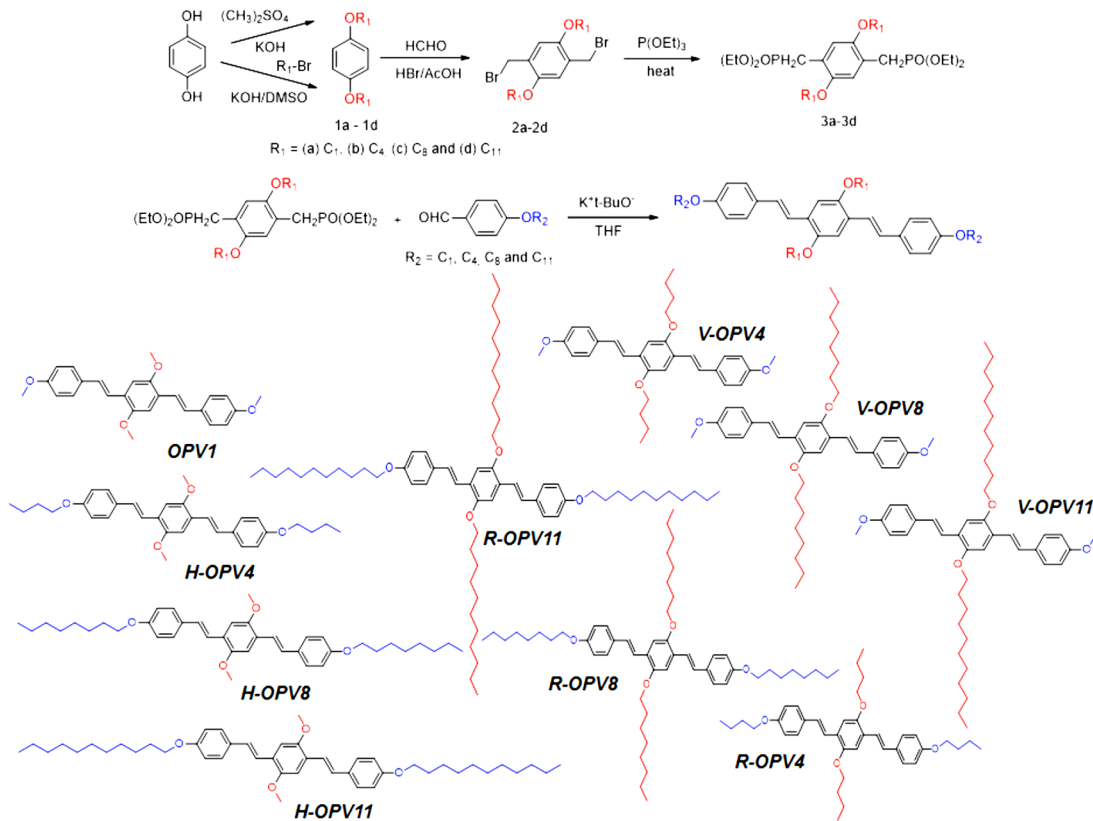


**Figure 1.** (a) Spatial expansion of  $\pi$ -conjugated OPVs horizontally (along the X axis), vertically (along the Y axis) and radially (along both the X and Y axes). The red solid part represents the rigid aromatic OPV  $\pi$ -core, and the gray lines and fillings around the  $\pi$ -core represent the aliphatic content. (b) Role of planarity in the  $\text{CH}/\pi$  interactions and LC mesophase of OPVs.

### Scheme 1. Synthesis of Horizontally, Vertically, and Radially Expanded OPVs



hydrocarbon skeleton oligo(phenylenevinylene) (OPV) chromophores.<sup>24,25</sup> Preliminary investigations of the single-crystal structures of these OPVs revealed that multiarm  $\text{CH}/\pi$ /

hydrogen-bonding interactions facilitate the formation of chiral nematic ring banded self-assemblies.<sup>26,27</sup> Efforts were also made to trace the roles of hydrocarbon- and fluorocarbon-tailed

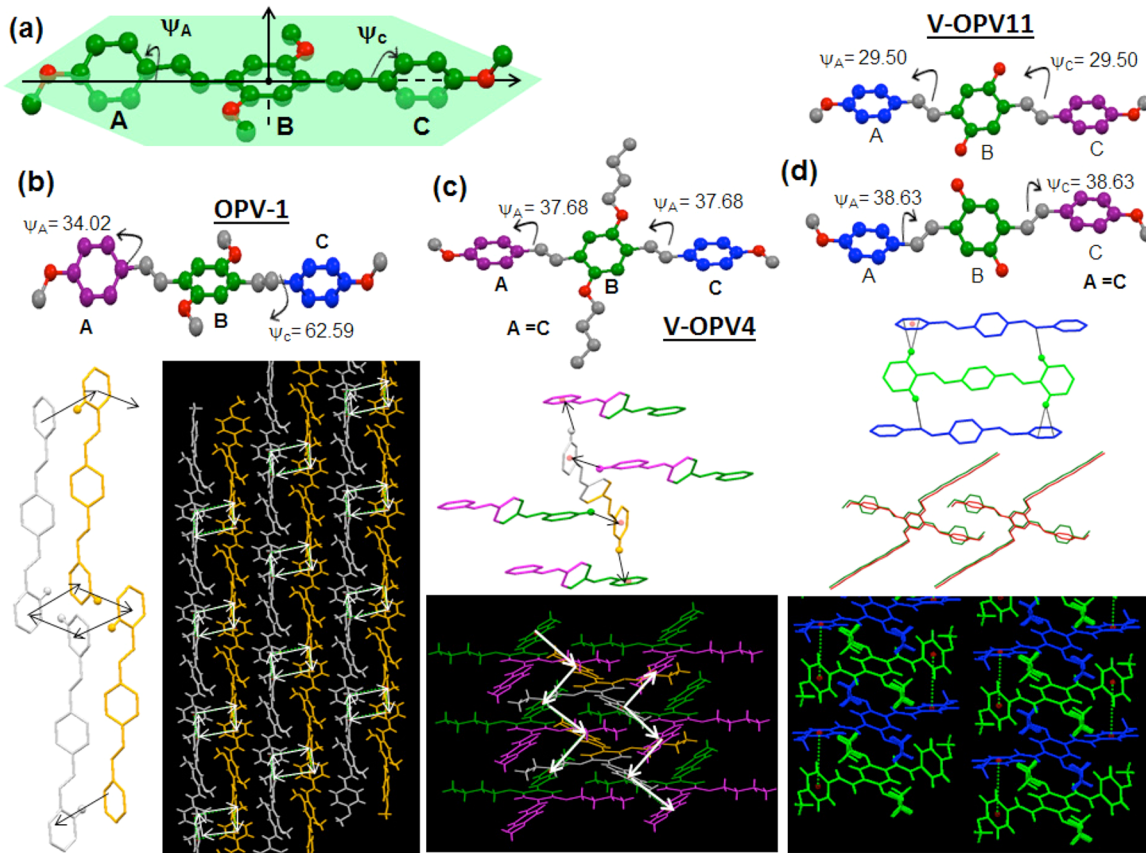


**Figure 2.** (a) Aromatic ring distortion in the OPV backbone. (b–d) Single-crystal X-ray structures of (b) OPV1, (c) V-OPV4, and (d) V-OPV11 and their three-dimensional packing. In (d), the long alkyl tails in the middle aromatic rings have been omitted for better representations of  $\psi_A$  and  $\psi_C$ .

OPVs in their smectic LC mesophases.<sup>28</sup> These studies facilitated the making of helical segmented OPV polymers<sup>29</sup> and their organogel photonic switches.<sup>30</sup> A few other groups have also reported the single-crystal structures of OPVs to understand their emission characteristics.<sup>31–35</sup> Ajayaghosh and co-workers reported the conversion of OPV chromophores into organogels and supramolecular helical self-assemblies.<sup>36–39</sup> Meijer and co-workers developed unique quadruple-hydrogen-bonded OPV assemblies for making supramolecular polymers and organogels.<sup>40–43</sup> These studies emphasized the importance of the development of aromatic  $\pi$ -conjugated assemblies. However, until now there has been no effort to trace the secondary forces that control the mesophase assemblies of OPV  $\pi$ -conjugates and their solid-state luminescence properties. Addressing this multitask problem is highly dependent on the following criteria: (i) the appropriate design of  $\pi$ -conjugates with sufficient structural diversity; (ii) the ability of the  $\pi$ -conjugates to produce good-quality single crystals to allow the study of the secondary interactions; and (iii) the ability of the  $\pi$ -conjugates to produce self-assembled mesophases and so on.

The present work is one of the first attempts to trace the secondary forces in  $\pi$ -conjugated chromophores with planar or nonplanar geometries in a single system, and it also aims to establish the correlation between the  $\pi$ -conjugated chemical structures and the mesophase self-assemblies. For this purpose, spatially expandable OPV molecules having an identical aromatic  $\pi$ -core and variable aliphatic content were developed through tailor-made approaches (see Figure 1). Three series of

horizontally, vertically, and radially expanded OPVs (H-OPVs, V-OPVs, and R-OPVs, respectively) were synthesized by varying the aliphatic content along the X axis, the Y axis, and both the X and Y axes, respectively (see Figure 1). Large numbers of single-crystal structures of these OPVs were resolved, allowing us to trace the non-covalent forces that dictate the chromophore packing in the 3D crystal lattices. Efforts were made to establish the correlation between molecular planarity, aromatic  $\pi$ -stacking, and CH/ $\pi$  hydrogen-bonding interactions in  $\pi$ -conjugated OPV systems. Furthermore, the roles of these secondary interactions on the LC mesophase assemblies and lamellar packing were also studied by absolute solid-state quantum yield determinations and time-resolved fluorescence decay dynamics studies. Preliminary efforts were also made to employ an OPV molecule as the active layer in an FET. The present approach provides new insight into the precise molecular arrangements of planar and nonplanar geometries, mesophase alignment, and solid-state characteristics more specifically based on OPV chromophores.

## RESULTS AND DISCUSSION

**Synthesis and Crystal Structures of OPVs.** Three series of horizontally, vertically, and radially expanded OPVs were synthesized by varying the aliphatic content along the X axis, the Y axis, and both the X and Y axes, respectively (see Figure 1). The H-OPVs, V-OPVs, and R-OPVs were synthesized as shown in Scheme 1. The length and position of the alkyl chains were varied from C<sub>1</sub> to C<sub>11</sub> in both R<sub>1</sub> and R<sub>2</sub> in the OPV core.

In the first series,  $R_1$  was fixed as  $\text{CH}_3$  and  $R_2$  was varied as  $\text{CH}_3$ ,  $\text{C}_4\text{H}_9$ ,  $\text{C}_8\text{H}_{17}$ , and  $\text{C}_{11}\text{H}_{23}$  to make H-OPVs (see Scheme 1). In the second series,  $R_2$  was fixed as  $\text{CH}_3$  and  $R_1$  was varied as  $\text{CH}_3$ ,  $\text{C}_4\text{H}_9$ ,  $\text{C}_8\text{H}_{17}$ , and  $\text{C}_{11}\text{H}_{23}$  to make V-OPVs. Retaining  $R_1 = R_2$  and varying the number of carbon atoms as 1, 4, 8, and 11 ( $\text{CH}_3$ ,  $\text{C}_4\text{H}_9$ ,  $\text{C}_8\text{H}_{17}$ , and  $\text{C}_{11}\text{H}_{23}$ ) afforded the series of R-OPVs. The basic OPV structure having all four sides with methoxy substitution is named as OPV1 ( $R_1 = R_2 = \text{CH}_3$ ). The other OPVs are named as H-OPV $n$ , V-OPV $n$ , and R-OPV $n$ , where  $n$  represents the number of carbons in the alkyl chains varied in that particular series. All of these OPVs were characterized by  $^1\text{H}$  and  $^{13}\text{C}$  NMR, FT-IR, MALDI-TOF-TOF, and elemental analysis, and these details are provided in the Supporting Information. H-OPV4 and V-OPV4; H-OPV8 and V-OPV8; and H-OPV11 and V-OPV11 are structural isomers that differ only at the point of alkyl chain attachment in the  $\pi$ -core.

The crystallographic data for the OPV molecules are provided in the Supporting Information (see Tables ST1 and ST2). OPV structures are broadly classified into two types with respect to their planarity. The angles  $\psi_A$  and  $\psi_C$  subtended by two terminal rings on the central aromatic ring are shown in Figure 2a. The three phenyl rings have been labeled as A, B, and C for easy identification. For a planar molecule  $\psi_A = \psi_C \approx 0$ , and for the nonplanar OPVs  $\psi_A \neq \psi_C \neq 0$  or  $\psi_A = \psi_C \neq 0$ . The unit cell for OPV1 is shown in Figure 2b (see SF-1 and SF-2 in the Supporting Information for more information). In OPV1, the two terminal aromatic rings A and C have moved out of the plane of the central aromatic ring B in opposite directions, giving rise to a nonplanar structure (see Figure 2b). The torsional angles of the central aromatic ring with the terminal aromatic rings were measured to be  $\psi_A = 34.02^\circ$  and  $\psi_C = 62.59^\circ$ . Intermolecular close contacts revealed that a total of four CH/ $\pi$  interactions are present between neighboring molecules (see SF-3). The CH/ $\pi$  interactions are validated by the four parameters,  $d_{c-x}$ ,  $\theta$ ,  $\phi$ , and  $d_{H-p}$  (see Table ST3), as reported earlier.<sup>27,28,42,43</sup> The CH/ $\pi$  interactions are involved between aryl C–H donors and aryl rings as  $\pi$ -acceptors in a perpendicular orientation in the edge-to-face arrangement (see SF-1). The three-dimensional packing of these molecules shows head-to-tail arrangements that are interlocked by four CH/ $\pi$  interactions in a square-planar fashion (shown by the arrows in Figure 2b). The interlocking in a head-to-tail fashion among rings A and C produces long one-dimensional molecular stacks. The CH/ $\pi$  interactions were found to be present only along the molecular axis in each stack, and there are no interactions between the adjacent stacks.

Vertical expansion of the alkyl carbon atoms in V-OPV4 produces an orthorhombic crystal system, and the molecule belongs to the centrosymmetric space group  $Pbca$  (see Figure 2c and SF-4). In V-OPV4, the two terminal aromatic rings have been moved out of the plane in the same direction (unlike in OPV1; see Figure 2b), giving rise to a nonplanar geometry. The angles subtended by the terminal aromatic rings on the central aromatic ring are equal and were measured to be  $\psi_A = \psi_C = 37.68^\circ$ . The three-dimensional packing revealed an extended network of CH/ $\pi$  interactions in the zigzag chains (see SF-4). The CH/ $\pi$  interactions are directed in an angular fashion, subtending an angle of  $104.8^\circ$  relative to each other. These interactions are locked through four identical CH/ $\pi$  interactions involving  $\text{Ar}-\text{C}-\text{H}_6$  as the donor and the terminal phenyl ring as the  $\pi$ -acceptor system (see Figure 2c). As the alkyl chain length further was increased in the vertical

expansion, the V-OPV11 molecules were found as molecular dimers (see Figure 2d). Each molecular dimer consists of two molecules with different aromatic geometries (see SF-5). The two terminal aromatic rings in the first molecule have been moved out of the plane of the middle aromatic ring equally in the same direction, giving rise to a nonplanar molecule. The torsional angles were measured to be  $29.50^\circ$  for one such aromatic system (top molecule in Figure 2d). In the second molecule, the torsional angles between the terminal and central rings were measured to be  $38.63^\circ$  (bottom molecules in Figure 2d). The three-dimensional packing revealed that the molecules are arranged right on the top of each other, giving rise to lamellar packing (see SF-5). Each green molecule present in the stack is locked by two blue molecules (top and bottom) at either side (see Figure 2d, shown by dotted lines). The CH/ $\pi$  interactions are directed in a linear fashion (see SF-6) rather than a square-planar or angular fashion, as observed in their shorter counterpart V-OPV4. These interactions reveal that each central molecule exhibits CH/ $\pi$  interactions with an aromatic ring as well as C=C double bonds (see SF-6 and Table ST3).

The radially extended OPV molecule R-OPV8 is shown in SF-7. The middle aromatic ring in R-OPV8 has been moved out of the plane constituted by the terminal rings. Both torsional angles of the central aromatic ring with respect to the terminal aromatic rings were found to be  $45.71^\circ$ . One of the terminal  $\text{C}_8$  alkyl tails has two carbons in a gauche conformation. The octyl chains attached to the terminal rings are laid along the molecular axis, whereas those attached to the central aromatic rings protrude above and below the molecular plane. CH/ $\pi$  interactions between  $\text{H}_{22}$  (donor) and the central aryl ring (acceptor), between aryl  $\text{H}_2$  (donor) and the  $\text{C}_{12}=\text{C}_{15}$  double bond (acceptor), and between  $\text{H}_{35A}$  (donor) and  $\text{C}_4=\text{C}_7$  (acceptor) were observed (see SF-8). The three-dimensional structure of these molecules shows lamellar-type packing in which the molecules are interdigitized in a parallel fashion along the long molecular axis. The R-OPV11 molecule was found to be planar, and there are no CH/ $\pi$  interactions between aryl H atoms and aryl rings. However, weak CH/ $\pi$  interactions between the  $\text{R}-\text{CH}_2\text{O}$  hydrogens and aryl rings were observed.<sup>27</sup> Among the horizontal OPVs, only the H-OPV11 molecule produced a single-crystal, and its structure was found to be planar with no C–H/ $\pi$  interactions.<sup>27</sup> OPVs such as H-OPV4, H-OPV8, V-OPV8, and R-OPV4 did not produce good-quality crystals.

#### CH/ $\pi$ Hydrogen Bonding and Planarity of the $\pi$ -Core.

Single-crystal X-ray diffraction (XRD) analysis revealed that both the length of the alkyl chains and their point of attachment in the aromatic core as well as the planarity of the  $\pi$ -backbone play important roles in determining the solid-state packing of the chromophores. Furthermore, it was observed that the planar molecules are devoid of CH/ $\pi$  interactions. On the other hand, the nonplanar molecules exhibited strong CH/ $\pi$  interactions. In all cases except in R-OPV11, the CH/ $\pi$  interactions occurred between aryl C–H donors and aryl rings as acceptors. In order to establish a direct correlation between the planarity of the molecules and the CH/ $\pi$  interactions, the angles  $\psi_A$  and  $\psi_C$  were plotted, as shown in Figure 3. In OPV1, the two terminal aromatic rings have been moved out of the plane of the middle aromatic ring in opposite directions, giving rise to a nonplanar molecule. In contrast to OPV1, the two terminal aromatic rings in V-OPV4 have been moved out of the plane of the central ring in the same direction,

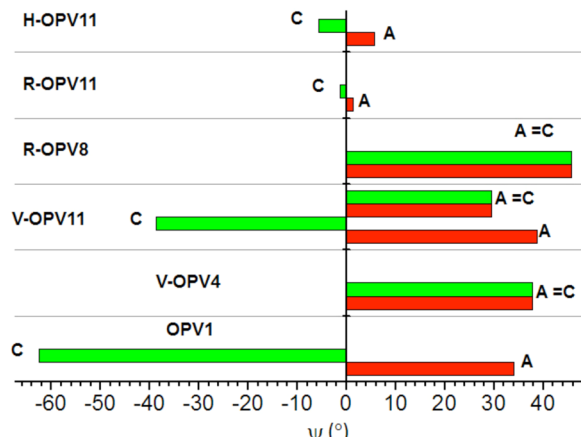


Figure 3. Plot of the torsional angles  $\psi_A$  and  $\psi_C$  in the OPVs.

giving rise to a nonplanar molecule. Interestingly, V-OPV11 exists as molecular dimers with different projections of terminal aryl rings. In the first molecule, the two terminal aromatic rings have been moved out of the plane equally in the same direction, giving rise to a nonplanar molecule. In the second molecule, aromatic ring B occupies the middle plane and the terminal rings have been pushed in two different parallel planes on either side by a distance of 1.85 Å (see Figure 2). This clearly indicates that the vertical expansion of OPV chromophores favors a nonplanar conformation. This nonplanar geometry promotes the V-OPVs to self-organize via CH/ $\pi$  interactions. In the case of radial expansion, R-OPV8 is nonplanar and shows CH/ $\pi$  interactions. On the other hand, the longer-chain-substituted R-OPV11 shows CH/ $\pi$  interactions with the R-CH<sub>2</sub>O hydrogens rather than aryl hydrogens. The H-OPV11 molecule is planar, and there are no CH/ $\pi$  interactions. The relationship between planarity and CH/ $\pi$  interactions in the OPVs are summarized in Table 1. The vertical expansion makes

Table 1. Correlation between the Planarity of the Molecule, CH/ $\pi$  Hydrogen Bonding, and Types of Assemblies in the Expanded OPV Chromophores

type	planarity	CH/ $\pi$	$\pi-\pi$	self-assembly
H-OPV	planar	no	no	crystalline to liquid-crystalline
V-OPV	nonplanar	yes	no	crystalline (only)
R-OPV	nonplanar ( $<C_8$ ) planar ( $>C_8$ )	yes no	no	crystalline to lamellar lamellar

the OPVs nonplanar, and the CH/ $\pi$  interactions interlock the molecules. On the other hand, the horizontally expanded OPV molecules show a planar geometry, and the CH/ $\pi$  interactions are completely absent in the crystal lattices. In the case of radially expanded OPVs, the shorter C<sub>8</sub> chains make the OPV nonplanar, whereas the longer C<sub>11</sub> chains in the central ring are projected perpendicular to the planar aromatic  $\pi$ -core. The Ar-OCH<sub>2</sub>-R protons act as donors and exhibit weak CH/ $\pi$  interactions. In order to solve this unusual trend in the R-OPVs; another radial OPV was tailor-made with C<sub>8</sub> substitution on the middle ring and C<sub>11</sub> substitution on the terminal aryl rings (see SF-8).<sup>28</sup> This unequal radial expansion produced a planar geometry without any CH/ $\pi$  interactions. Thus, it may be concluded that radial expansion in the OPVs produces a nonplanar geometry with shorter chains, whereas the molecule

becomes planar with substitution of longer alkyl chains along the molecular axis (see Table 1).

**Enthalpies, Mesophase Assemblies, and Layered Structures.** The OPV molecules were subjected to thermal analysis and polarized light microscopy (PLM) analysis to study their LC mesophases. The OPVs were subjected to differential scanning calorimetry (DSC) analysis with 10°/min heating and cooling cycles, and their thermograms are shown in the SF-9 and SF-10. The basic OPV1 molecule showed single melting and crystallization peaks in the heating and cooling cycles with respect to crystalline solids. The R-OPVs showed two melting transitions in the heating and cooling cycles. These transitions resemble the thermal behaviors of the LC samples (see SF-10).

For instance, the peaks at 100 and 160 °C in R-OPV4 in the heating cycles were assigned to the Crys-LC and LC-Iso transitions. These transitions were reversible in the subsequent cooling cycles. Horizontal expansion of the OPV from H-OPV4 to H-OPV8 did not change the crystalline nature; however, substitution with the longer alkyl tail (in H-OPV11) produced two peaks with respect to LC features (see SF-10). On the other hand, the V-OPVs were found to be crystalline solids (see SF-10). The thermal data for all of the OPVs in the respective heating and cooling cycles are summarized in the Table ST-4. To find a general relationship describing how these thermal properties changed with variation of the peripheral alkyl chain substitution, the enthalpies of melting ( $\Delta H_m$ ) and crystallization ( $\Delta H_c$ ) transitions were plotted against the types of OPVs, as shown in Figures 4a and 4b (for the melting and crystallization temperatures, see SF-10). Highly packed structures need more energy to melt and expel more energy during crystallization in the heating and cooling cycles, respectively. The parent OPV-1 molecule with methoxy substitution on the periphery showed lower melting and crystallization enthalpies compared with the other analogues, which suggests that the introduction of alkyl chain substitution on the rigid OPV core enhances the molecular packing for higher crystallinity. Among the three series, the H-OPVs were found to be highly crystalline with higher enthalpy values. The V-OPVs showed lower  $\Delta H_m$  and  $\Delta H_c$  irrespective of the chain length. The R-OPVs showed a slight increase in melting enthalpy with increasing chain length of the alkyl units. Thus, among the three OPVs, the H-OPVs have a much higher tendency to pack, as reflected in their higher enthalpies for melting and crystallization processes.

The above thermal analysis suggested that substitution of longer alkyl chains along the horizontal direction of the aromatic core tends to increase the packing among these classes of expanded OPV chromophores. In contrast, the introduction of long alkyl chains in the vertical direction (i.e., along the short molecular axis) destabilizes the molecular packing and lowers the enthalpies of transition. On the basis of the evidence from the crystal structures and enthalpy values, a model has been drawn for the OPV chromophore arrangements with respect to their horizontal, vertical, and radial expansion (see Figure 4c). The nonplanar, rigid OPV-1 molecule exhibits zigzag packing (see SF-3) to produce a weakly crystalline material. The horizontal expansion of the OPVs makes the  $\pi$ -core become planar, which facilitates the packing of the OPVs to give a highly crystalline material. The vertical expansion produces a nonplanar  $\pi$ -core, which was found to be less preferable for packing in the solid state. The radial expansion in both the X and Y directions in the OPV core results in a change in the  $\pi$ -core from nonplanar to planar. The planar R-OPV11 molecule

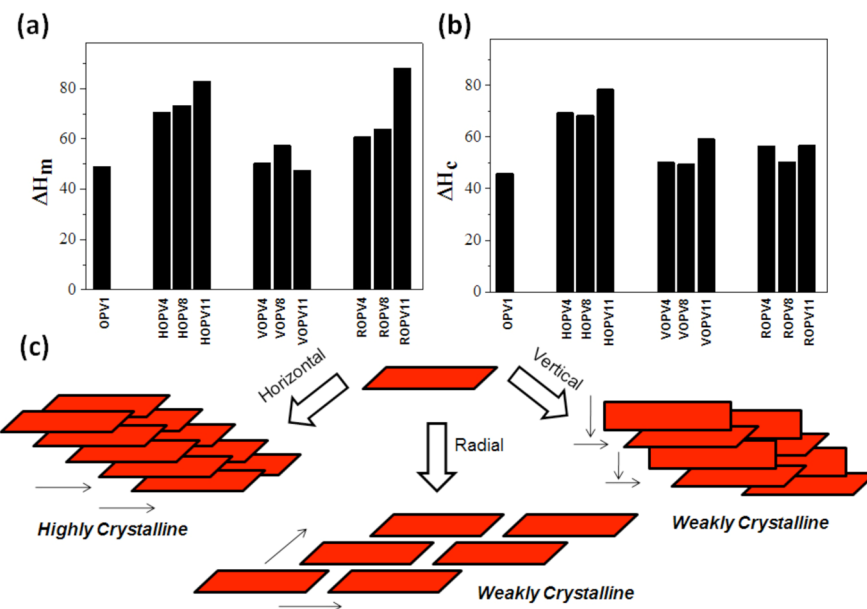


**Figure 4.** (a, b) Enthalpies of (a) melting and (b) crystallization of OPVs. (c) Schematic representation of packing of the OPV molecules with horizontal, vertical, and radial expansion.

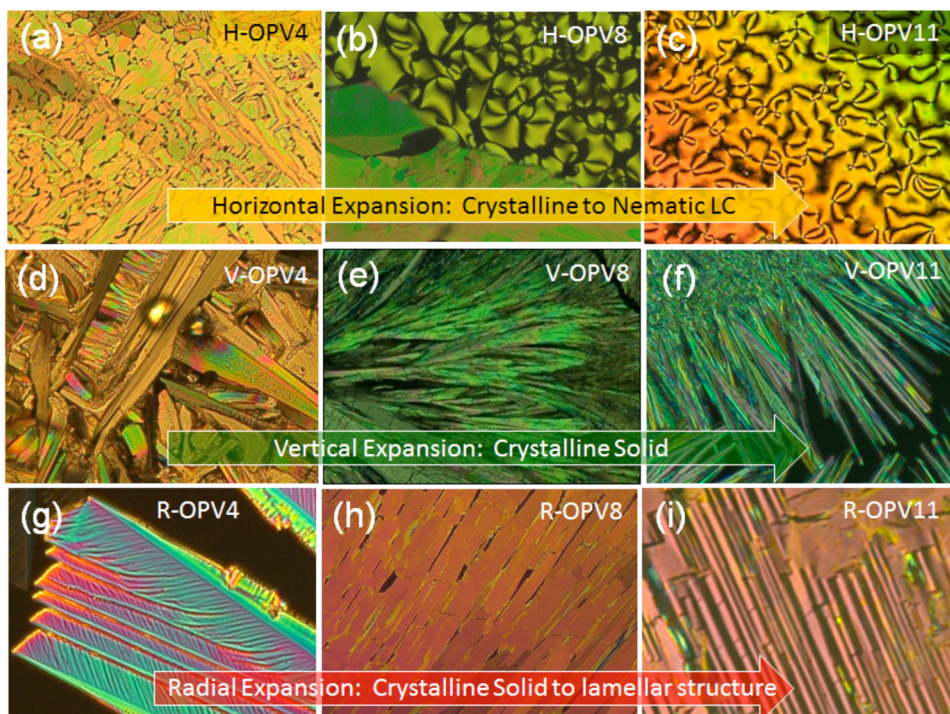


**Figure 5.** PLM images of OPVs in the cooling cycle at 10°C/min.

produces higher crystallinity compared with the nonplanar R-OPV4 and R-OPV8 molecules. Thus, planarity of the aromatic  $\pi$ -core is essential for producing highly crystalline OPV materials.

To study the temperature dependence of the LC texture, the OPVs were subjected to PLM analysis with a programmable hot stage. The sample was placed on the glass substrate, heated to melt at 10 °C/min, and kept isothermally at 20 °C above their melting temperature for 2–3 min. The melt was subsequently cooled at 10 °C/min to capture the images using a high-resolution camera. The detailed temperature-

dependent LC textures of OPVs are given in SF-12 to SF-14, and a few representative PLM images are shown in Figure 5. OPV1 exhibited sharp needlelike nucleation at 212 °C, and the rapid growth of crystalline vectors resulted in the formation of typical crystalline images at room temperature (see SF-12). H-OPV4 exhibited growth patterns similar to those of crystalline solids (see Figure 5a and also SF-12). As the alkyl chain length increased further, the H-OPV8 molecule became LC in nature; however, the texture was mixed with crystalline textures (see the image in Figure 5b). H-OPV11 exhibited spherical droplets as nucleating sites, and these droplets quickly merged to

produce schlieren nematic LC textures (see Figure 5c). The PLM images of the V-OPVs showed crystalline textures irrespective of the alkyl chain length (see Figure 5d–f and SF-13). PLM images of R-OPVs showed layerlike textures (see Figure 5g–j). R-OPVC8C11 with unequal radial substitution also showed a leaflike LC growth pattern (see SF-14). Thus, the OPV chromophores produced different types of mesophase assemblies with respect to their chemical structure upon crystallization from the molten state.

Single crystals of organic molecules were grown in solution by slow evaporation of the solvent, whereas the LC mesophases (or crystalline textures) were obtained by a solvent-free melt crystallization process. Hence, it is important to correlate the OPV crystalline packing in these two independent processes to rationalize the similarities in the molecular self-organization of OPV chromophores. For this purpose, variable-temperature XRD patterns of the OPV samples were recorded for the powder samples and compared with the X-ray patterns simulated from their single-crystal structures.<sup>28</sup> Wide-angle XRD (WXRD) patterns of R-OPV8 are shown in Figure 6a (for

shown for R-OPV8 in Figure 6b). Comparison of Figure 6a and Figure 6b revealed that the two fundamental peaks in the experimental WXRD patterns belong to the 010 and 100 fundamental planes (see Figure 6c). The *d* spacings for all of the other peaks in the experimental XRD patterns at  $2\theta = 14.7^\circ$ ,  $16.5^\circ$ , and  $20.26^\circ$  were assigned to the 020, 200, and 030 lattice planes. The perfect match of the *d* spacings in the simulated and experimental XRD patterns supports the identical packing of the molecules in the single-crystal and powder samples. Similarly, comparison of the simulated and experimental XRD patterns of R-OPVC8C11 showed identical crystal packing in the single-crystal and powder samples (see SF-17). Thus, the layered crystalline arrangements in the PLM images of R-OPVs (see Figure 5) arose from the perfect lamellar ordering of the crystalline vectors during cooling from the melt.

On the basis of the above analysis, the overall trend in the mesophase assemblies of horizontally, vertically, and radially expanded OPVs are summarized in Table 1. Increasing the alkyl chain length along the horizontal direction induces LC properties in OPVs. The H-OPVs resemble the dumbbell shape along the direction of the  $\pi$ -core and can rapidly spin around their long molecular axis (see Figure 1a). This spinning movement is important for the generation of stable LC mesophases, as spinning suppresses crystallization at lower temperatures. This point is further supported by the planarity of the molecule, as is evident from the single-crystal structure of H-OPV11. Furthermore, there are no secondary interactions (either CH/ $\pi$  or  $\pi$ - $\pi$ ); thus, these molecules can freely rotate to produce nematic LC domains. The introduction of long alkyl chains in the direction perpendicular to the aromatic core (in V-OPVs) suppresses the molecular spinning, leading to destabilization of the LC phase. The suppression of spinning is further evident from the nonplanar nature of V-OPV4 and V-OPV11 and the existence of strong CH/ $\pi$  interactions in their crystal lattices. The equal expansion of OPVs in both the *X* and *Y* directions results in the intermediate state that produces lamellar textures in R-OPV8 and R-OPV11. Thus, by means of the present design strategy, one can easily fine-tune the OPV thermal properties as well as their LC mesophases depending upon the appropriate selection of the length of the alkyl chains and their point of attachment to the OPV  $\pi$ -core.

**PLQYs, Fluorescence Decay, and Charge Mobility.** The absorption and emission spectra of OPVs on a quartz substrate are shown in Figure 7a–c. The absorption maxima of all of the OPVs were found in the range of 400 to 450 nm. The OPVs exhibited emission maxima in the range of 504 to 535 nm. The emission spectra of the H-OPV series showed a slight red shift compared with the other samples. This is attributed to the planar  $\pi$ -structure and highly packed crystalline domains in the H-OPVs.

Highly packed  $\pi$ -conjugated molecules show higher enthalpies in melting and crystallization transitions with respect to ordered structures. In the present investigation, the OPV molecules have different enthalpy values with respect to their variation in crystal packing in the solid state. As a result, these OPVs are expected to show differences in their solid-state photoluminescence quantum yields (PLQYs). The exciton created in the photoexcitation process would be expected to decay much faster in the highly packed structures compared with the weakly packed analogues.<sup>25</sup> To test this hypothesis, all three series of expanded OPV structures were subjected to absolute solid-state PLQY measurements using an integrating

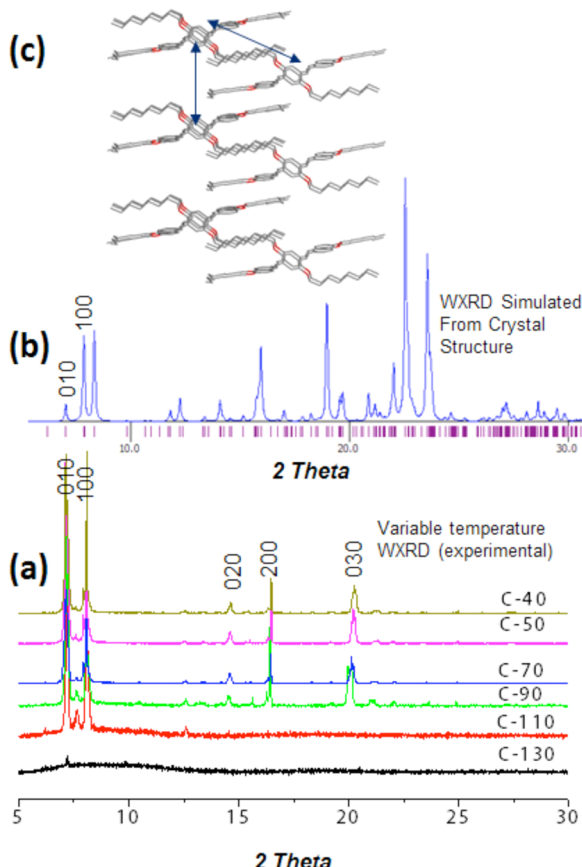


**Figure 6.** (a) Variable-temperature wide-angle X-ray diffraction patterns of R-OPV8. (b) Simulated WXRD pattern of R-OPV8. (c) Crystal packing of R-OPV8 molecules viewed through the *c* crystallographic axis.

other OPVs, see SF-15 and SF-16). In the molten state, the R-OPV8 sample did not show any diffraction at 130 °C (see Figure 6a), and sharp crystalline patterns appeared in the subsequent cooling. At lower temperatures, other sharp peaks appeared at higher angles with respect to the long-range packing of the molecules. The powder XRD patterns of these samples were simulated from their single-crystal structures, as

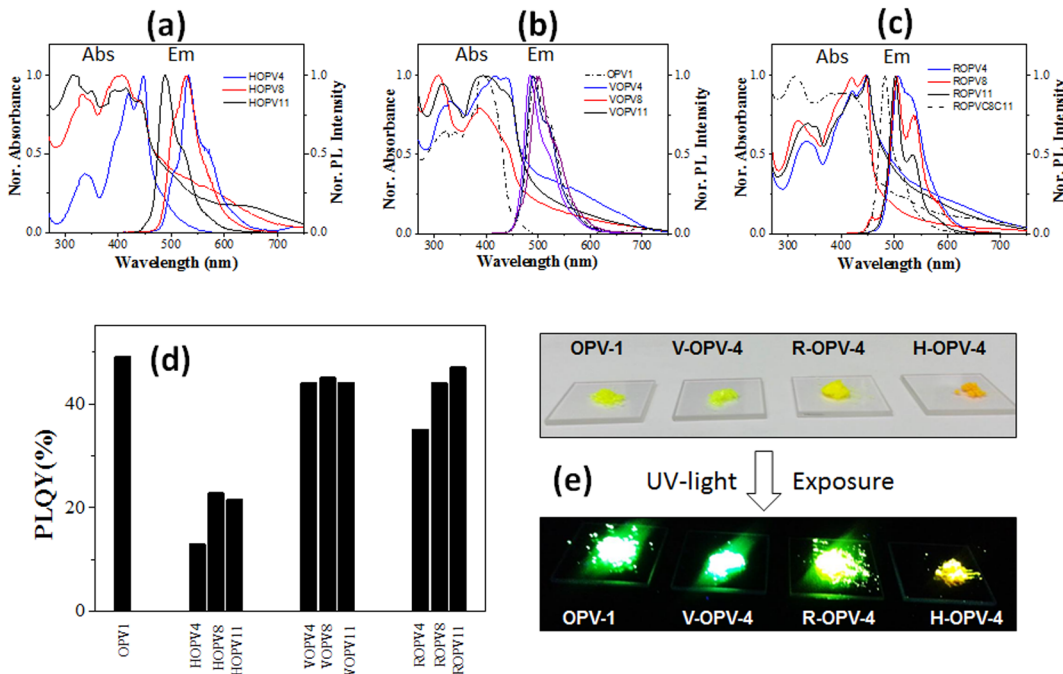


**Figure 7.** Absorbance and emission spectra of (a) the H-OPV series, (b) the V-OPV series, and (c) the R-OPV series. The data for OPV1 data are merged with V-OPV series. Emission spectra were recorded using an excitation wavelength of 400 nm. (d) Absolute solid-state photoluminescence quantum yields of OPVs measured by integrating sphere techniques. (e) Photographs of OPV samples on a quartz plate before and after exposure to UV light.

**Table 2. Fluorescence Lifetimes of OPVs in Thin Films<sup>a</sup>**

sample	$\tau_1$ (ns)	$\tau_2$ (ns)	$A_1$	$A_2$	$\chi^2$	$\tau_{avg}$ (ns) <sup>b</sup>
OPV1	$1.14 \pm 0.017$	$2.55 \pm 0.007$	21.47	78.53	1.07	2.02
H-OPV4	$0.84 \pm 0.009$	$1.50 \pm 0.017$	73.18	26.82	1.01	0.96
V-OPV4	$0.72 \pm 0.007$	$1.70 \pm 0.017$	79.45	20.55	1.1	0.80
R-OPV4	$0.74 \pm 0.015$	$1.71 \pm 0.008$	48.46	51.54	1.12	1.04
H-OPV11	$0.88 \pm 0.012$	$1.68 \pm 0.016$	71.92	28.08	1.05	1.02
V-OPV11	$1.21 \pm 0.01$	$2.47 \pm 0.02$	77.31	22.69	1.05	1.36
R-OPV11	$1.10 \pm 0.013$	$1.70 \pm 0.042$	79.88	20.12	1.2	1.20

<sup>a</sup>A nano-LED with a wavelength of 371 nm was used as the excitation source. <sup>b</sup>The details of the average lifetime calculations are given in ST-5 in the Supporting Information.

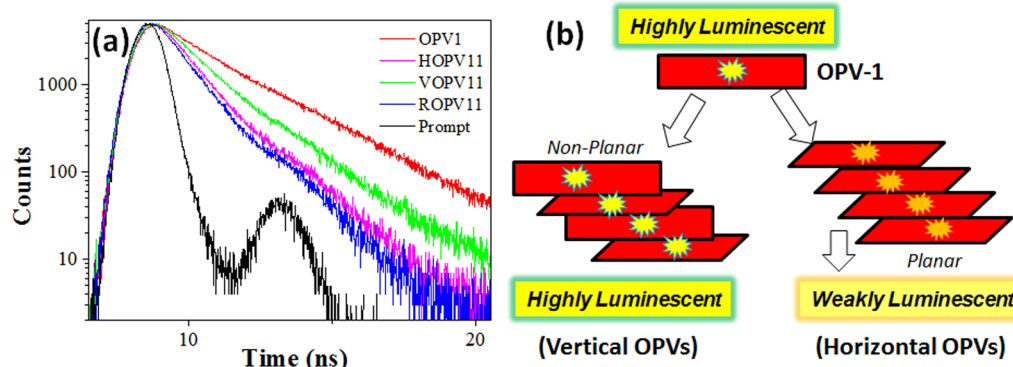


**Figure 8.** (a) TCSPC decay profiles of OPVs. (b) Model for the decay of excitons in the OPV packed structures.

sphere setup. This method was developed previously by Palsson and Monkma<sup>44</sup> using a Horiba Jobin Yvon Fluorolog-3 instrument and was recently employed by us in measurements on semicrystalline  $\pi$ -conjugated OPV segmented polymers to validate the effects of their solid-state ordering

on their emission characteristics.<sup>30</sup> The obtained PLQYs of the OPVs (Figure 7d) were 16–48%, which are very good for OPV chromophore systems.<sup>30</sup> Among all of the OPV molecules, the parent OPV1 molecule with methoxy substitution showed highest PLQY (48%). The H-OPV series showed lowest

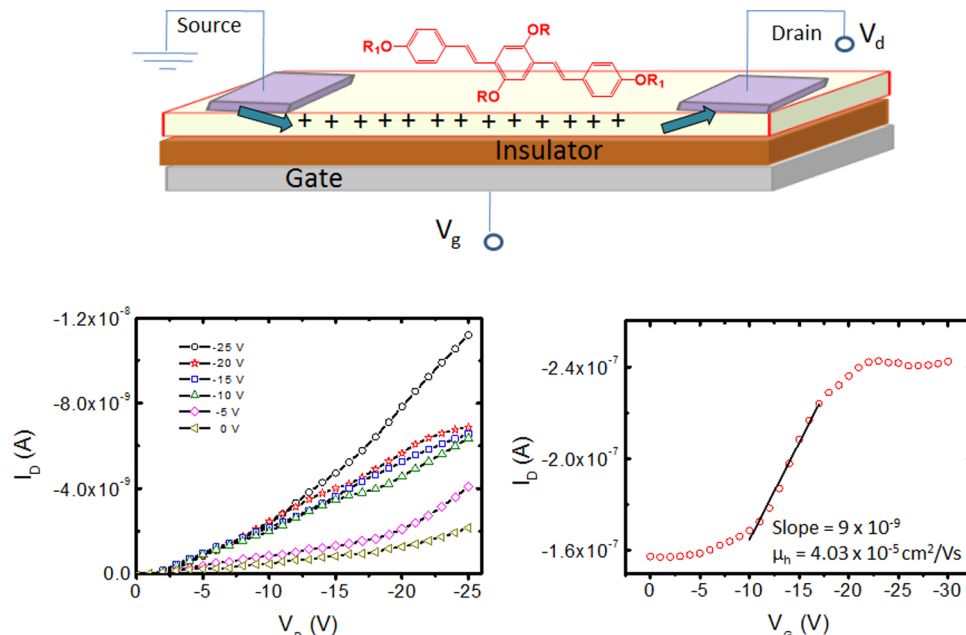


**Figure 9.** Field-effect transistor measurements for an H-OPV11 film.

PLQYs compared with all of the other OPVs. Comparison of the PLQY data in Figure 7d with the enthalpies of packing in OPVs (see Figure 4a,b) revealed that the highly packed H-OPV series showed low PLQYs compared with the weakly packed V-OPVs and R-OPVs. The PLQY data in Figure 7d follow just the opposite trend of the enthalpies of packing in OPVs. This trend is attributed to the luminescence quenching in the ordered crystalline domains of OPV chromophores. The photographs of the OPV samples upon exposure to UV-light photoexcitation are shown in Figure 7e. The weakly crystalline OPV1, V-OPV4, and R-OPV4 molecules show bright green emission, whereas the highly crystalline H-OPV4 showed less intense yellow emission. These observations support the trend in the PLQYs shown in Figure 7d.

To further understand the excited-state fluorescence dynamics of OPV chromophores, OPV1 and the OPVs having  $C_4$  and  $C_{11}$  carbon chains were subjected to fluorescence lifetime analysis by the time-correlated single-photon counting (TCSPC) technique. The OPVs were excited with a 371 nm nano-LED excitation source, and the decay profiles were collected at their emission maxima. The decay profiles were fitted to biexponential decay functions, and their decay lifetimes are given in Table 2. The decay profiles in Figure 8a reveal that the OPV1 shows very slow decay (stable emission) compared with the  $C_{11}$  series OPVs (for the  $C_4$  series, see SF-18). The decay profiles decreased in the order OPV1 > V-OPV11 > R-OPV11 = H-OPV11. This trend is similar to that of their PLQYs (see Figure 7c) but opposite to that of their enthalpies of melting and crystallization (see Figure 4a,b).

The first fast decay was attributed to the OPV chromophore, and the subsequent second slow decay typically represents the difference in their self-assembled molecular states.<sup>25</sup> The first decay times  $\tau_1$  were found to be in the range of 0.6–1.2 ns, which is typically observed for OPV chromophores.<sup>27</sup> The second decay times  $\tau_2$  were found to vary widely with respect to the type of the OPV self-assembly.<sup>25</sup> The weakly packed and high-PLQY samples OPV1 and V-OPV11 showed  $\tau_2 = 2.5$  ns, whereas the highly ordered and low-PLQY samples H-OPV11 and R-OPV11 showed  $\tau_2 = 1.7$  ns. Thus, the highly packed H-

OPV molecules showed low PLQYs as a result of the fast decay of the exciton in the crystalline domain (see the model in Figure 8b). Weakly packed OPV materials do not have perfect pathways for exciton diffusion; as a result, the V-OPVs and R-OPVs were turned into highly luminescent materials. Thus, a very good correlation of the geometry of the molecules with their packing ability and solid-state photophysical characteristics has been established in  $\pi$ -conjugated OPV molecules.

As a proof of concept, an FET was fabricated using H-OPV11, and FET measurements were done for a drop-cast film. The plots of drain current ( $I_D$ ) versus drain voltage ( $V_D$ ) for various applied gate voltage ( $V_G$ ) are shown in Figure 9. The output characteristic curves show a clear linear regime and drain current modulation as a function of gate voltage. The field-effect mobility was calculated using linear and saturated regime methods. It should be noted that the saturation was not perfect, and hence, the highest drain voltage used was taken as  $V_D$  while carrying out the transfer characteristic  $I$ – $V$  measurements.<sup>45,46</sup> The threshold voltage ( $V_{TH}$ ) was calculated from the plot of  $I_D^{1/2}$  versus  $V_G$ . The charge carrier mobilities calculated using both the linear and saturated regime methods showed that the mobility in the drop-cast film of H-OPV11 was on the order of  $10^{-5} \text{ cm}^2 \text{ V}^{-1} \text{ s}^{-1}$  (linear regime,  $-4.2 \times 10^{-5} \text{ cm}^2 \text{ V}^{-1} \text{ s}^{-1}$ ; saturation regime,  $-7.7 \times 10^{-5} \text{ cm}^2 \text{ V}^{-1} \text{ s}^{-1}$ ). The on/off ratio and  $V_{TH}$  value were obtained as 5.01 and  $-9.0$  V, respectively (see SF-19). The above preliminary device results show that the newly designed OPVs provide a useful materials approach for molecular devices.

## CONCLUSION

The present investigation provides in-depth knowledge on the roles of molecular planarity,  $\text{CH}/\pi$  hydrogen bonding, and peripheral alkyl chain substitution on the molecular self-assembly of  $\pi$ -conjugates. New series of horizontally, vertically, and radially expanded OPV chromophores were custom-synthesized for the above purpose. The single-crystal structures of these OPVs revealed that planar molecules were found to be devoid of  $\text{C}-\text{H}/\pi$  secondary interactions. PLM studies

confirmed that these planar and horizontally expanded OPVs produced nematic LC mesophases. The nonplanar molecules (radially and vertically expanded OPVs) exhibited strong CH/ $\pi$  interactions and were found to be crystalline solids. Variable-temperature X-ray diffraction analysis established the origin of lamellar structures in the R-OPVs. Planar OPV conjugates showed high enthalpies of melting and crystallization transitions with respect to highly packed structures. The absolute PLQYs of the highly packed OPV chromophores were found to be much lower than those of the weakly packed analogues. The rationale behind this trend was further supported by time-resolved fluorescent decay dynamics analysis using the TCSPC method. The excitons generated by the photoexcitation process undergo fast decay in the ordered and highly packed H-OPV series, resulting in their low PLQYs. An FET device was constructed for H-OPV11 to study the hole transport charge carrier mobility. The expanded  $\pi$ -conjugated approach demonstrated herein is not restricted only to OPV chromophores and in principle could be expanded to a large number of other  $\pi$ -conjugated materials. The present investigation opens up a new avenue for understanding the molecular self-organization in  $\pi$ -conjugates and also may serve as a seed for appropriate structural design that is required for the future material development for molecular devices.

## ■ ASSOCIATED CONTENT

### Supporting Information

Synthetic details, single-crystal parameters, calculation of CH/ $\pi$  parameters, TGA and DSC data, a table containing the thermal data, PLM images, and NMR and MALDI-TOF spectra of the OPVs and intermediates. This material is available free of charge via the Internet at <http://pubs.acs.org>. The crystallographic information files (cif) of the single-crystal structures have been deposited at the Cambridge Crystallographic Data Centre. CCDC 1020078–1020082, 839244, and 839245 contain the supplementary crystallographic data for this paper. These data can be obtained free of charge from the Cambridge Crystallographic Data Centre via [www.ccdc.cam.ac.uk/data\\_request/cif](http://www.ccdc.cam.ac.uk/data_request/cif).

## ■ AUTHOR INFORMATION

### Corresponding Author

\*E-mail: jayakannan@iiserpune.ac.in. Fax: +91-20-2590 8187.

### Author Contributions

All authors contributed equally.

### Notes

The authors declare no competing financial interest.

## ■ ACKNOWLEDGMENTS

The authors thank the Department of Science and Technology (DST), New Delhi, India, for a research grant under the SERB Scheme (SB/OC/OM-10/2014) and MHRD, New Delhi, for research funding under the FAST Scheme for the Centre of Sustainable Energy at IISER-Pune. K.N. thanks UGC, New Delhi, India, for a research fellowship. The authors thank Mr. Arul S. Kashmir and Dr. K. Krishnamoorthy at NCL-Pune for OFET data and useful discussions, Dr. R. Boomishankar and Dr. Arvind K Gupta for their help in resolving the single-crystal structures, and the CSIR TAPSUN (NWP 54) Programme for the fabrication facilities.

## ■ REFERENCES

- (1) Akcelrud, L. Electroluminescent Polymers. *Prog. Polym. Sci.* **2003**, *28*, 875–962.
- (2) Gunes, S.; Neugebauer, H.; Sariciftci, N. S. Conjugated Polymer-Based Organic Solar Cells. *Chem. Rev.* **2007**, *107*, 1324–1338.
- (3) Sun, Y.; Liu, Y.; Zhu, D. Advances in Organic Field-Effect Transistors. *J. Mater. Chem.* **2005**, *15*, 53–65.
- (4) Wang, C.; Dong, H.; Hu, W.; Liu, Y.; Zhu, D. Semiconducting  $\pi$ -Conjugated Systems in Field-Effect Transistors: A Material Odyssey of Organic Electronics. *Chem. Rev.* **2012**, *112*, 2208–2267.
- (5) Grimme, S. Do Special Noncovalent  $\pi$ – $\pi$  Stacking Interactions Really Exist? *Angew. Chem., Int. Ed.* **2008**, *47*, 3430–3434.
- (6) Payne, M. M.; Parkin, S. R.; Anthony, J. E.; Kuo, C. C.; Jackson, T. N. Organic Field-Effect Transistors from Solution-Deposited Functionalized Acenes with Mobilities as High as  $1\text{ cm}^2/\text{V}\cdot\text{s}$ . *J. Am. Chem. Soc.* **2005**, *127*, 4986–4987.
- (7) Garnier, F. Organic-Based Electronics à la Carte. *Acc. Chem. Res.* **1999**, *32*, 209–215.
- (8) Ackermann, C.-V.; Ackermann, J.; Brisset, H.; Kawamura, K.; Yoshimoto, N.; Raynal, P.; Kassmi, A. E.; Fages, F.  $\alpha,\omega$ -Distyryl Oligothiophenes: High Mobility Semiconductors for Environmentally Stable Organic Thin Film Transistors. *J. Am. Chem. Soc.* **2005**, *127*, 16346–16347.
- (9) Meng, H.; Sun, F.; Goldfinger, M. B.; Jaycox, Z. L.; Marshall, W. J.; Blackman, G. S. High-Performance, Stable Organic Thin-Film Field-Effect Transistors Based on Bis-5'-alkylthiophen-2'-yl-2,6-anthracene Semiconductors. *J. Am. Chem. Soc.* **2005**, *127*, 2406–2407.
- (10) Torrent, M. M.; Durkut, M.; Hadley, P.; Ribas, X.; Rovira, C. High Mobility of Dithiophene-Tetrathiafulvalene Single-Crystal Organic Field Effect Transistors. *J. Am. Chem. Soc.* **2004**, *126*, 984–985.
- (11) Sokolov, A. N.; Atahan-Evrenk, S.; Mondal, R.; Akkerman, H. B.; Sanchez-Carrera, R. S.; Granados-Focil, S.; Schrier, J.; Mannsfeld, S. C. B.; Zoombelt, A. P.; Bao, Z.; Aspuru-Guzik, A.; et al. From Computational Discovery to Experimental Characterization of a High Hole Mobility Organic Crystal. *Nat. Commun.* **2011**, *2*, No. 437.
- (12) Nishida, J.; Kumaki, D.; Tokito, S.; Yamashita, Y. High Performance n- and p-Type Field-Effect Transistors Based on Tetrathiafulvalene Derivatives. *J. Am. Chem. Soc.* **2006**, *128*, 9598–9599.
- (13) Nishida, J.; Ando, S.; Yamaguchi, J.; Itaka, K.; Koinuma, H.; Tada, H.; Tokito, S.; Yamashita, Y. High-Performance Organic Field-Effect Transistors Based on  $\pi$ -Extended Tetrathiafulvalene Derivatives. *J. Am. Chem. Soc.* **2005**, *127*, 10142–10143.
- (14) Curtis, M. D.; Cao, J.; Kampf, J. W. Solid-State Packing of Conjugated Oligomers: From  $\pi$ -Stacks to the Herringbone Structure. *J. Am. Chem. Soc.* **2004**, *126*, 4318–4328.
- (15) Holmes, D.; Kumaraswamy, S.; Matzger, A. J.; Vollhardt, K. P. C. On the Nature of Nonplanarity in the [N]Phenylenes. *Chem.—Eur. J.* **1999**, *5*, 3399–3412.
- (16) Sokolov, A. N.; Friscic, T.; MacGillivray, L. R. Enforced Face-to-Face Stacking of Organic Semiconductor Building Blocks within Hydrogen-Bonded Molecular Cocrystals. *J. Am. Chem. Soc.* **2006**, *128*, 2806–2807.
- (17) Xie, Z.; Yang, B.; Xie, W.; Liu, L.; Shen, F.; Wang, H.; Yang, X.; Wang, Z.; Li, Y.; Hanif, M.; et al. A Class of Nonplanar Conjugated Compounds with Aggregation-Induced Emission: Structural and Optical Properties of 2,5-Diphenyl-1,4-distyrylbenzene Derivatives with All Cis Double Bonds. *J. Phys. Chem. B* **2006**, *110*, 20993–21000.
- (18) Stalmach, U.; Schollmeyer, D.; Meier, H. Single-Crystal Structures of Model Compounds for Poly(2,5-dialkoxy-1,4-phenylenevinylene). *Chem. Mater.* **1999**, *11*, 2103–2106.
- (19) Vande Velde, C. M. L.; Chen, L.-J.; Baeke, J. K.; Moens, M.; Dieltiens, P.; Geise, H. J.; Zeller, M.; Hunter, A. D.; Blockhuys, F. The Influence of the Side Chain Length on  $-\text{OCH}_3$ – $\pi$  Interactions Determining the Crystal Packing of Four Substituted 1,4-Bis( $\alpha$ -styryl)benzenes. *Cryst. Growth Des.* **2004**, *4*, 823–830.

- (20) Vande Velde, C. M. L.; Baeke, J. K.; Geise, H. J.; Blockhuys, F. (*E,E*)-2,5-Dipropoxy-1,4-bis[2-(2,4,6-trimethoxyphenyl)ethenyl]-benzene. *Acta Crystallogr.* **2005**, *C61*, o284–o287.
- (21) O'Neill, M.; Kelly, S. M. Ordered Materials for Organic Electronics and Photonics. *Adv. Mater.* **2011**, *23*, 566–584.
- (22) O'Neill, M.; Kelly, S. M. Liquid Crystals for Charge Transport, Luminescence, and Photonics. *Adv. Mater.* **2003**, *15*, 1135–1145.
- (23) Shimizu, Y.; Oikawa, K.; Nakayama, K.; Guillon, D. Mesophase Semiconductors in Field Effect Transistors. *J. Mater. Chem.* **2007**, *17*, 4223–4229.
- (24) Amrutha, S. R.; Jayakannan, M. Supramolecular Ring Banded Prototype Liquid Crystalline Oligo(phenylenevinylene). *J. Phys. Chem. B* **2009**, *113*, 5083–5091.
- (25) Singh, H.; Balamurugan, A.; Jayakannan, M. Solid State Assemblies and Photophysical Characteristics of Linear and Bent-Core  $\pi$ -Conjugated Oligophenylenevinylenes. *ACS Appl. Mater. Interfaces* **2013**, *5*, 5578–5591.
- (26) Goel, M.; Jayakannan, M. Supramolecular Liquid Crystalline  $\pi$ -Conjugates: The Role of Aromatic  $\pi$ -Stacking and van der Waals Forces on the Molecular Self-Assembly of Oligophenylenevinylenes. *J. Phys. Chem. B* **2010**, *114*, 12508–12519.
- (27) Goel, M.; Jayakannan, M. CH/ $\pi$  Interaction Guided Molecular Self-Assembly in  $\pi$ -Conjugated Oligomers. *Chem.—Eur. J.* **2012**, *18*, 2867–2874.
- (28) Goel, M.; Jayakannan, M. Herringbone and Helical Self-Assembly of  $\pi$ -Conjugated Molecules in Solid State through CH/ $\pi$  Hydrogen Bond. *Chem.—Eur. J.* **2012**, *18*, 11987–11993.
- (29) Goel, M.; Narasimha, K.; Jayakannan, M. Helical Self-Assemblies of Segmented Poly(phenylenevinylene)s and their Hierarchical Donor–Acceptor Complexes. *Macromolecules* **2014**, *47*, 2592–2603.
- (30) Narasimha, K.; Jayakannan, M.  $\pi$ -Conjugated Polymer Anisotropic Organogel Nanofibrous Assemblies for Thermoresponsive Photonic Switches. *ACS Appl. Mater. Interfaces* **2014**, *6*, 19385–19396.
- (31) Gill, R. E.; Meetsma, A.; Hadzioannou, G. Two Novel Thermotropic Liquid Crystalline Substituted Oligo(*p*-phenylenevinylene)s: Single Crystal X-ray Determination of an All-*trans* Oligomeric PPV. *Adv. Mater.* **1996**, *8*, 212–214.
- (32) Bartholomew, G. P.; Bu, X.; Bazan, G. C. Preferential Cocrystallization among Distyrylbenzene Derivatives. *Chem. Mater.* **2000**, *12*, 2311–2318.
- (33) Gao, F.; Liao, Q.; Xu, Z. Z.; Yue, Y. H.; Wang, Q.; Zhang, H. L.; Fu, H. B. Strong Two-Photon Excited Fluorescence and Stimulated Emission from an Organic Single Crystal of an Oligo(phenylenevinylene). *Angew. Chem., Int. Ed.* **2010**, *49*, 732–735.
- (34) Detert, H.; Schollmeyer, D.; Sugiono, E. Synthesis, Structure and Solvatochromism of the Emission of Cyano-Substituted Oligo(phenylenevinylene)s. *Eur. J. Org. Chem.* **2001**, 2927–2938.
- (35) Sierra, C. A.; Lahti, P. M. A Photoluminescent, Segmented Oligo-Polyphenylenevinylene Copolymer with Hydrogen-Bonding Pendant Chains. *Chem. Mater.* **2004**, *16*, 55–61.
- (36) Ajayaghosh, A.; Vijayakumar, C.; Varghese, R.; George, S. J. Cholesterol-Aided Supramolecular Control over Chromophore Packing: Twisted and Coiled Helices with Distinct Optical, Chiroptical, and Morphological Features. *Angew. Chem., Int. Ed.* **2006**, *45*, 456–460.
- (37) Babu, S. S.; Praveen, V. K.; Prasanthkumar, S.; Ajayaghosh, A. Self-Assembly of Oligo(*para*-phenylenevinylene)s through Arene-Perfluoroarene Interactions:  $\pi$  Gels with Longitudinally Controlled Fiber Growth and Supramolecular Exciplex-Mediated Enhanced Emission. *Chem.—Eur. J.* **2008**, *14*, 9577–9584.
- (38) Hirai, Y.; Babu, S. S.; Praveen, V. K.; Yasuda, T.; Ajayaghosh, A.; Kato, T. Anisotropic Self-Assembly of Photoluminescent Oligo(*p*-phenylenevinylene) Derivatives in Liquid Crystals: An Effective Strategy for the Macroscopic Alignment of  $\pi$ -Gels. *Adv. Mater.* **2009**, *21*, 4029–4033.
- (39) Babu, S. S.; Praveen, V. K.; Ajayaghosh, A. Functional  $\pi$ -Gelators and Their Applications. *Chem. Rev.* **2014**, *114*, 1973–2129.
- (40) Janssen, P. G. A.; Meeuwenoord, N.; Marel, G. V.; Jabbari-Farouj, S.; Schoot, P. V. D.; Surin, M.; Tomovic, Z.; Meijer, E. W.; Schenning, A. P. H. J. ssPNA Templated Assembly of Oligo(*p*-phenylenevinylene)s. *Chem. Commun.* **2010**, *46*, 109–111.
- (41) Jonkheijm, P.; Schoot, P. V. D.; Schenning, A. P. H. J.; Meijer, E. W. Probing the Solvent-Assisted Nucleation Pathway in Chemical Self-Assembly. *Science* **2006**, *313*, 80–83.
- (42) Schenning, A. P. H. J.; Jonkheijm, P.; Peeters, E.; Meijer, E. W. Hierarchical Order in Supramolecular Assemblies of Hydrogen-Bonded Oligo(*p*-phenylene vinylene)s. *J. Am. Chem. Soc.* **2001**, *123*, 409–416.
- (43) Herrikhuyzen, J. V.; Asha, S. K.; Schenning, A. P. H. J.; Meijer, E. W. Synthesis of n-Type Perylene Bisimide Derivatives and Their Orthogonal Self-Assembly with p-Type Oligo(*p*-phenylene vinylene)s. *J. Am. Chem. Soc.* **2004**, *126*, 10021–10027.
- (44) Palsson, L.-O.; Monkma, A. P. Measurements of Solid-State Photoluminescence Quantum Yields of Films Using a Fluorimeter. *Adv. Mater.* **2002**, *14*, 757–758.
- (45) Arulkashmir, A.; Mahale, R. Y.; Dharmapurikar, S. S.; Jangid, M. K.; Krishnamoorthy, K. Supramolecular Interaction Facilitated Small Molecule Films for Organic Field Effect Transistors. *Polym. Chem.* **2012**, *3*, 1641–1646.
- (46) Dharmapurikar, S. S.; Arulkashmir, A.; Das, C.; Muddellu, P.; Krishnamoorthy, K. Enhanced Hole Carrier Transport Due to Increased Intermolecular Contacts in Small Molecule Based Field Effect Transistors. *ACS Appl. Mater. Interfaces* **2013**, *5*, 7086–7093.